Green and low-cost synthesis of N and P double doped porous carbon derived from Sonchus arvensis L for simultaneous electrochemical detection of ascorbic acid, dopamine and uric acid

Qiaoqian Sun
Chongqing University
Xiaolong Liang
Chongqing University
Zuohua Liu
Chongqing University
Gong Li
Chongqing University
Yijiao Zhang
Chongqing University
Siwei Jin
Chongqing University
Hongchen Pu
Chongqing University
Miao Yin
Chongqing University
Jinyin Yu
Chongqing University
Wanying Yan
Chongqing University
Huanbao Fa (huanbaofa@cqu.edu.cn)
Chongqing University
Wei Yin
Analytical and Testing Center of Chongqing University

Research Article

Keywords: Ascorbic acid, Dopamine, Uric acid, Electrochemical simultaneous detection, Sonchus arvensis L

Posted Date: February 9th, 2023

DOI: https://doi.org/10.21203/rs.3.rs-2558200/v1

Abstract

N and P double doped porous carbon derived from Sonchus arvensis L at different carbonization temperatures (700 °C, 800 °C and 900 °C) were prepared by a simple one-step activation pyrolysis for the simultaneous electrochemical detection of AA, DA and UA. Compared with SaL-700 and SaL-900, the Sal-800 show excellent electrochemical sensing ability. Therefore, further electrochemical sensing studies were carried out by using SaL-800. The linear range of AA was 200-6000 μM., the sensitivity was 0.06 $\mu A \cdot \mu M^{-1} \cdot cm^{-2}$, and the detection limit was 76 μM (S/N=3). The sensitivity of DA was 9.81 $\mu A \cdot \mu M^{-1} \cdot cm^{-2}$ (0.5-20 μM) and 39.69 $\mu A \cdot \mu M^{-1} \cdot cm^{-2}$ (20-90 μM), and the detection limit was 0.11 μM (S/N=3). The sensitivity of UA was 0.81 $\mu A \cdot \mu M^{-1} \cdot cm^{-2}$ (10-100 μM) and 4.05 $\mu A \cdot \mu M^{-1} \cdot cm^{-2}$ (100-900 μM), and the detection limit was 2.70 μM (S/N=3). In addition, satisfactory results have been obtained for the determination of AA, DA and UA in normal human serum, which provides a new research direction for the construction of electrochemical sensors in the future.

1. Introduction

Ascorbic acid (AA), known as vitamin C, is distributed in plants and animals. As an antioxidant, AA can stabilize the color of food and the performance of cosmetics, so it is widely used in food, medicine and other fields. The main function of AA in human body is to prevent cancer and improve immunity. Its deficiency can lead to scurvy, collagen metabolism disorder and even infertility [1–3]. Dopamine (DA) plays an important role in the central nervous system, kidney, hormone and cardiovascular system. Measuring the level of DA in extracellular fluid has important clinical significance for monitoring the process of neurotransmission and diagnosing Parkinson's disease [4–6]. Uric acid (UA) is the decisive product of purine metabolism in human body. The change of uric acid concentration is closely related to purine metabolism. The determination of UA is very important in the treatment of severe hepatitis, hyperuricemia, renal failure and other diseases caused by abnormal purine metabolism [7–9]. AA, DA and UA usually coexist in human body fluid, the oxidation potentials of them are close on the traditional electrode, which is easy to cause the overlap of oxidation peaks [10–12]. Therefore, it is essential to develop electrode modified materials with high sensitivity and selectivity for the simultaneous determination of AA, DA and UA.

Compared with traditional detection methods (such as capillary electrophoresis, fluorescence spectroscopy, liquid chromatography and chemiluminescence spectroscopy), which are time-consuming, complex and expensive, electrochemical detection technology arises with its advantages of fast, sensitivity and simple operation. In recent years, different electrode modification materials have been developed to improve the sensitivity and selectivity of the electrode, which can be roughly divided into carbon nanotubes (CNTs) [13–15], graphene (GR) [16–20], polymers [21–24], ionic liquids (ILs) [25–27] and nanoparticles (NPs) [28–30]. Among them, biomass carbon materials have attracted great interest because of unique properties, such as low-cost precursors, simple and environmentally friendly preparation processes, ultra-high specific surface area and excellent chemical stability.

Biomass carbon materials with porous and heteroatom self-doping characteristics can be obtained by the carbonization of biomass precursors with natural porosity and rich elements at high temperature [31–33]. Porosity is an important index to evaluate biomass carbon materials, in order to obtain better porosity, physical or chemical activation is usually used in the process of preparing carbon materials. Notably, chemical activation with phosphoric acid can form micropores and mesopores in the carbon structure, thus greatly improving the porosity [34, 35]. Huang et al [36] synthesized N, P double doped porous carbon (CNP) derived from lotus leaves for simultaneous electrochemical detection of AA, DA and UA, achieved good detection results. Vediyappan veeramani et al [37] prepared biomass derived activated carbon (ACs) for the simultaneous detection of AA, DA and UA, the ACs have better catalytic activity than reduced graphene oxide. Li et al [38] prepared carbon nanoplates with ground cherry to construct an advanced electrochemical sensor (BG-CNPs/GCE). In addition to the detection of hydrogen peroxide (H_2O_2), tryptophan (TRP), purine and other small molecules, it can also realize the simultaneous detection of AA, DA and UA. These researches demonstrate that biomass-derived functional porous carbons as novel electrode materials are very promising.

Sonchus arvensis L (SaL) is a perennial herb, rich in amino acids and vitamins, which can be used as medicine and food. It has a strong reproductive ability and global footprint. In this study, with Sonchus arvensis L as precursor and phosphoric acid as activator, N and P double doped porous carbon derived from Sonchus arvensis L at different carbonization temperatures were synthesized by a simple one-step activation pyrolysis method. The porous carbon materials synthesized at 700°C, 800°C and 900°C are denoted as SaL-700, SaL-800 and SaL-900, respectively. The preparation and detection process of SaL-800 are shown in the Scheme 1. In simultaneous determination of AA, DA and UA, the acceptable linear range and lower detection limit are obtained, and the as-prepared sensor was successfully applied for detecting AA, DA and UA in human serum.

2. Experimental

2.1 Materials and apparatus

The Supplementary information (Scheme 1) provides a detailed description of the chemicals and reagents, as well as instruments utilized, and the measurements conducted.

2.2 Synthesis of SaL carbon materials

Sonchus arvensis L came from Huxi campus of Chongqing University in Chongqing. The picked Sonchus arvensis L was washed several times with deionized water, dried at 80℃ for 12 h, and crushed into powder. Divide the powder into three equal parts, 5g each. Mix three parts of powder with 50% phosphoric acid in the impregnation ratio of 1:2.5, stir with magnetic force for 1 h, and soak for 12 h, respectively. The soaked samples were placed in a tubular furnace, heated at 700 ℃, 800 ℃ and 900 ℃, with a heating rate of 5 ℃/min, and pyrolyzed at high temperature for 2 h in N_2 atmosphere to obtain carbon materials labeled as SaL-700, SaL-800 and SaL-900, respectively. Then ground in agate mortar for 30

minutes, soaked in 2 M HCl for 12 hours, filtered and washed with deionized water for many times until the pH value of the filtrate was neutral, and dried in the oven to obtain the final carbon material.

2.3 Preparation of SaL/GCE

The glassy carbon electrode was polished with 0.3 and 0.05 μm alumina slurry, ultrasonic treated in ethanol and deionized water for 5 minutes, and then dried in air. Add 2 mg SaL-700, SaL-800 and SaL-900 carbon materials into 1 mL distilled water and disperse them with ultrasound for 30 min to obtain a uniformly dispersed suspension. Transfer an appropriate amount of suspension drops and apply them to the center of GCE. Dry them naturally at room temperature to obtain carbon modified electrode marked as SaL/GCE.

3. Results And Discussion

3.1 Characterization studies

The surface area and pore properties of carbon materials were analyzed by nitrogen adsorption-desorption analysis. Figure 1A exhibits the N_2 adsorption-desorption isotherms, the BET surface area of SaL-800 is the best, about 695.25 m^2/g, while SaL-700 and SaL-900 are 358.21 m^2/g and 468.22 m^2/g, respectively. The highest surface area can be obtained at 800℃, indicating that the best activation temperature is 800℃. Figure 1B shows the pore size distribution of SaL-800. The pore size is mainly distributed at 3.94 nm and 12.58 nm, which proves that SaL-800 has mesoporous properties. SaL-800 with high surface area and mesoporous structure can provide more active sites, improve ion migration and promote redox reaction, which is very beneficial to electroanalysis [39].

The Raman spectrums are exhibited in Fig. 1C. There are two obvious peaks at 1330 cm^{-1} and 1580 cm^{-1}, corresponding to the D band of disordered carbon and the G band of graphite carbon, respectively. Generally speaking, the relative strength ratio (ID/IG) of D band and G band is proportional to the number of defect sites of carbon materials [40, 41]. The relative strength ratio (ID/IG) of SaL-700, SaL-800 and SaL-900 were 0.933, 1.040 and 0.944, respectively. The result shows that SaL-800 has the high-density defect site, which can provide more active adsorption sites and is conducive to electrocatalysis. Moreover, it was further proved that the optimum activation temperature of SaL was 800℃.

Figure 1D shows the XRD pattern of SaL-800 in which two broad peaks are observed at around 23.4°and 43.7°corresponding to (002) and (100) planes of amorphous carbon, which indicating SaL-800 has amorphous properties [42].

The morphology of SaL-800 carbon material was characterized by scanning electron microscopy (SEM). As demonstrated in Fig. 2A-C, SaL-800 presents loose porous structure, which is conducive to increase the specific surface area and provide more active adsorption sites. Moreover, the porous structure is conducive to the transmission of electrolyte molecules. Figure 2D reveals elemental mapping of the SaL-800, the C, N, O and P elements are uniformly and continuously distributed in it, indicating that N and P

were successfully doped. N elements may mainly come from the carbonization of nitrogenous bases in SaL and P from the activation of phosphoric acid [36].

The surface chemical properties of SaL-800 were also investigated by the X-ray photoelectron spectroscopy (XPS). As shown in Fig. 3A, the SaL-800 is consisted of the C, O, N and P elements, and the relative atom percentages of C, O, N and P in SaL-800 are 76.42%, 15.90%, 2.67% and 5.01%, respectively, which once again suggested successful incorporation of N and P into the SaL-800. The high resolution fitted C1s spectrum (Fig. 3B) is deconvoluted into carbon peaks in different chemical environments. The peaks at 284.8 eV, 285.4 eV, 286.3 eV and 289.3 eV correspond to C = C, C-C, C-OH and C = O, respectively. The N1s spectrum (Fig. 3C) shows four different peaks, indicating the presence of pyridinic nitrogen (398.2 eV), pyrrolic nitrogen (399.9 eV), graphitic nitrogen (401.2 eV) and oxidized nitrogen (402.8 eV). Among them, pyridinic nitrogen and pyrrolic nitrogen contribute to increase the active site and improving the catalytic activity [43]. The P2p spectrum (Fig. 3D) has two main peaks at 132.8 eV and 133.6 eV, which are attributed to P-C and P-N bond, respectively. In conclusion, N and P elements in SaL-800 form active functional groups through different combinations, which will be beneficial to improve the electrocatalytic performance [36].

3.2 Electrochemical characteristic

Figure 4A shows the cyclic voltammograms (CV) in the 5.0 mM $K_3[Fe(CN)_6]$ and 0.1 M KCl mixed solution, and Fig. 4B shows the differential pulse voltammograms (DPV) in the mixed solution containing 500 μM AA, 50 μM DA and 50 μM UA at different activation temperatures. The current of SaL-800 is significantly better than that of SaL-700 and SaL-900 (Fig. 4A). When AA, DA and UA are detected simultaneously, SaL-800 still has excellent selectivity and conductivity (Fig. 4B). The results are consistent with BET and Raman. It is confirmed again that 800°C is the best activation temperature of SaL.

The cyclic voltammetry analysis of Bare GCE and SaL-800/GCE is shown in Fig. 4C. The current of Bare GCE is significantly lower than SaL-800/GCE, which indicates that the introduction of SaL-800 improves the conductivity of the electrode. Randles-Sevcik formula is introduced to calculate the effective working area (Aeff) of the electrode:

$$\mathrm{i_p} = \left(2.69 \times 10^5\right) \mathrm{n}^{\frac{3}{2}} \mathrm{A} * \mathrm{D}^{\frac{1}{2}} \mathrm{C} * \mathrm{V}^{1/2}$$

3.1

In the formula: n=1„ = 0.673×10-5 cm^2/s, C=5×10-6 mol/cm⁻, V=0.05 V/s.

Through calculation, the effective working areas of Bare GCE and SaL-800/GCE were 0.054 cm^2 and 0.064 cm^2, respectively, indicating that the SaL-800 with high specific surface area increases the effective

working area of the electrode and is conducive to improving the electrical analysis performance of the electrode.

Electrochemical impedance spectroscopy (EIS) analysis is shown in Fig. 4D. The upper left inset of Fig. 4D is an electrical equivalent fitting circuit diagram. The Rct value is calculated by the diameter of the high frequency semicircle in the ZsimpWin software fitting impedance diagram. The Rct of Bare GCE and SaL-800/GCE were 342 Ω and 70.62 Ω, respectively. The results are consistent with the cyclic voltammetry analysis, which further shows that the SaL-800 has good conductivity and electrochemical properties.

3.3 Electrocatalytic oxidation

The electrochemical sensing properties of different electrodes were investigated by CV and DPV to detect 500 μM AA, 50 μM DA and 50 μM UA simultaneously. As shown in Fig. 4E and Fig. 4F, Bare GCE all only has two peaks of DA and UA, however, three oxidation peaks are clearly observed by SaL-800/GCE, corresponding to AA, DA and UA, respectively. The peak currents and peak separations are significantly enhanced in DPV test, which indicates the detection sensitivity and selectivity of DPV are obviously superior to CV, so DPV is used in subsequent experiments. The DPV oxidation peak potentials of AA, DA and UA appeared at -28, 190 and 314 mV, respectively. And the peak separations of AA-DA, DA-UA and AA-UA were 218, 124 and 342 mV, respectively, which proves that SaL-800/GCE can realize the simultaneous electrochemical detection of AA, DA and UA.

3.4 Optimization of experimental conditions

For best experimental results, the coating amount of SaL-800 (V), pH value of PBS and enrichment time (T) were optimized in the mixed solution of 500 μM AA, 50 μM DA and 50 μM UA, as described in the Supplementary Information (S2) under the following experimental conditions: V = 6 μL, PH = 7 and T = 90s.

3.5 Effect of scan rate

The reaction kinetics of the electrode was investigated by studying the effect of scan rate. The scan rates of 10, 20, 30, 40, 50, 60, 70, 80, 90 and 100 mV were tested in the mixed solution of 500 μM AA, 50 μM DA and 50 μM UA. As shown in Fig. 5A the anodic peak currents of AA, DA and UA increase linearly with the scan rates and have good linear relationships with the scan rates (Fig. 5B), which proves that the electrocatalytic oxidation process of AA, DA and UA is controlled by adsorption.

3.6 Selectivity of AA, DA and UA detection by SaL-800/GCE

DPV was carried out for the simultaneous determination of AA, DA and UA in 0.1 M PBS (pH = 7). During the detection, the concentration of one analyte was changed, while the concentration of the other two analytes remained unchanged. As shown in Fig. 6A-F, the peak potentials of AA, DA and UA are well separated on SaL-800/GCE, and the anode peak current of each target detector is directly proportional to its concentration. The results show that changing the concentration of one target analyte has no

significant effect on the detection of the other two target analytes. The linear range of AA was 200–6000 μM, the sensitivity was 0.06 $\mu A \cdot \mu M^{-1} \cdot cm^{-2}$, and the detection limit was 76 μM (S/N = 3). The sensitivity of DA was 9.81 $\mu A \cdot \mu M^{-1} \cdot cm^{-2}$ (0.5–20 μM) and 39.69 $\mu A \cdot \mu M^{-1} \cdot cm^{-2}$ (20–90 μM), and the detection limit was 0.11 μM (S/N = 3). The sensitivity of UA was 0.81 $\mu A \cdot \mu M^{-1} \cdot cm^{-2}$ (10–100 μM) and 4.05 $\mu A \cdot \mu M^{-1} \cdot cm^{-2}$(100–900 μM), and the detection limit was 2.70 μM (S/N = 3). The analytical parameters of this study were compared to results from other reports in Table 1. The results show that SaL-800/GCE has relatively wide linear range and low detection limit.

Table 1
Performance comparison of different electrochemical sensors

Electrode	Linear range (μM)			LOD (μM)			References
	AA	DA	UA	AA	DA	UA	
HNP-PtTi	200–1000	4-500	100–1000	24.2	3.2	5.3	[44]
Au/RGO	240–1500	6.8–41	8.8–53	51	1.4	1.8	[45]
PtAu	103–165	24–384	21–336	103	20	21	[46]
Fe-M-PANI	10–300	10–300	10–300	6.5	9.8	5.3	[47]
CILE	50-7400	2-1500	2-220	20	1	1	[48]
Hnp-PtCu	25–800	4–20	10–70	17.5	2.8	5.70	[49]
OMC/Nafion	40–800	1–90	5–80	20	0.5	4.0	[50]
SaL-800	200–6000	0.5–90	10–900	76	0.11	2.70	This work

The detection performance of SaL-800/GCE for AA, DA and UA was also confirmed by increasing the concentration of three target analytes at the same time. With AA (500–2000 μM), DA (2–40 μM) and UA (8–40 μM), the anodic peaks of the three analytes (Fig. 7A) are still well separated, and there are good linear relationships between the peak currents of all analytes and their concentration (Fig. 7B-D). The detection limits of AA, DA and UA were 47.61, 1.14 and 1.86 μM (S/N = 3), respectively. In conclusion, SaL-800/GCE has high sensitivity and selectivity in the simultaneous detection of AA, DA and UA, which provides a broad prospect for the construction of high sensitivity and selectivity biosensors.

3.7 Selectivity, reproducibility and stability

Some organic compounds and inorganic ions may coexist with AA, DA and UA in real samples, such as glycine, glutamic acid, glucose, citric acid, K^+, Na^+, Cl^-, NO^{3-}, CO_3^{2-} and SO_4^{2-}. As shown in Fig. 8A, the current responses for AA (500 μM), DA (10 μM) and UA (10 μM) remain almost the same in the presence of aforementioned ions and compounds (100 μM), and the current variation are less than 10%. These

results indicate the SaL-800/GCE can effectively reduce the influence of possible interfering species and has good sensing performance for the detection of AA, DA and UA.

The reproducibility of SaL-800/GCE was evaluated by a series of 10 repeated measured responses to a mixture of AA (1 mM), DA (10 μM), and UA (10 μM). The relative standard deviations of peak anodic currents of AA, DA and UA were 1.44%, 1.95% and 1.68%, respectively (Fig. 8B). In addition, the SaL-800/GCE was stored at room temperature for two weeks, and then the electrode was tested. The peak currents of AA, DA and UA retained 98.55%, 98.06% and 98.34% of the initial currents, respectively. The above results show the SaL-800/GCE has excellent reproducibility and stability.

3.8 Real sample analysis

Normal human serum was selected as the real sample, and the actual effect of SaL-800/GCE on the simultaneous detection of AA, DA and UA was studied by standard addition method. Normal human serum samples were diluted 50 times with 0.1 M PBS (pH = 7) without another pretreatment. The recoveries of AA, DA and UA were in the range of 95.56%-105.90%, and the RSD was below 5% (Table 2), indicating that SaL-800/GCE can be effectively used for the simultaneous determination of AA, DA and UA in real samples.

Table 2
The recoveries of SaL/GCE in serum samples

Sample	Analytes	Added (μM)	Found (μM)	Recovery (%)	RSD (%)
Sample 1	AA	500.00	477.78	95.56	1.00
	DA	5.00	5.01	100.23	2.56
	UA	100.00	99.11	99.11	3.45
Sample 2	AA	1000.00	1050.00	105.00	1.95
	DA	10.00	9.84	98.38	1.32
	UA	200.00	211.79	105.90	2.85
Sample 3	AA	1500.00	1478.00	98.53	3.91
	DA	15.00	14.23	94.85	3.52
	UA	400.00	402.62	100.66	2.89

4. Conclusion

Using the green and environment-friendly Sonchus arvensis L plant as the precursor, N and P double doped endive carbon materials were obtained by a simple one-step phosphoric acid activation pyrolysis for the simultaneous detection of AA, DA and UA. Through the comparison of SaL-700, SaL-800 and SaL-

900, SaL-800 has the highest surface area and conductivity, and shows best catalytic activity for the electrooxidation of AA, DA and UA. The SaL-800/GCE sensor has wide linear range, low detection limit and high sensitivity. Thus, the low cost, environmentally friendly biomass carbon is an attractive candidate to fabricate electrochemical biosensors for the simultaneous determination of active biomolecules in bodies.

Declarations

Acknowledgements

This work was supported by the National Natural Science Foundation of China (No. 31101284), Chongqing Municipal Human Resources and Social Security Bureau (No. cx2020076), Chongqing Science and Technology Commission (No. CSTC2017shmsA100010), Chongqing Education Commission (KJZD-K202000101) and the Chongqing University Student Innovation Training Project (No. S202210611391, S202210611361).

References

1. Carita AC, Fonseca-Santos B, Shultz JD et al (2020) Review Article Vitamin C: One compound, several uses. Advances for delivery, efficiency and stability[J], vol 24. Nanotechnology, Biology, and Medicine, Nanomedicine, p 102117
2. Dhara K, Debiprosad RM (2019) Review on nanomaterials-enabled electrochemical sensors for ascorbic acid detection[J]. Anal Biochem 586:113415
3. Arrigoni O, De Tullio MC (2002) Ascorbic acid: much more than just an antioxidant[J]. Biochim et Biophys Acta (BBA)-General Subj 1569(1):1–9
4. Sajid M, Nazal MK, Mansha M et al (2016) Chemically modified electrodes for electrochemical detection of dopamine in the presence of uric acid and ascorbic acid: A review[J]. TRAC Trends Anal Chem 76:15–29
5. Jackowska K, Krysinski P (2013) New trends in the electrochemical sensing of dopamine[J]. Anal Bioanal Chem 405(11):3753–3771
6. Li J, Zhao J, Wei X (2009) A sensitive and selective sensor for dopamine determination based on a molecularly imprinted electropolymer of o-aminophenol[J]. Sens Actuators B 140(2):663–669
7. Wang QW, Wen X, Kong JM (2020) Recent Progress on Uric Acid Detection: A Review[J]. Crit Rev Anal Chem 50(4):359–375
8. Black CN, Bot M, Scheffer PG et al (2018) Uric acid in major depressive and anxiety disorders[J]. J Affect Disord 225:684–690
9. Nangare SN, Sangale PM, Patil AG et al (2021) Surface architectured metal organic frameworks-based biosensor for ultrasensitive detection of uric acid: Recent advancement and future perspectives[J]. Microchem J 169:106567

10. Zhu SY, Li HJ, Niu WX et al (2009) Simultaneous electrochemical determination of uric acid, dopamine, and ascorbic acid at single-walled carbon nanohorn modified glassy carbon electrode[J]. Biosens Bioelectron 25(4):940–943
11. Huang J, Liu Y, Hou H et al (2008) Simultaneous electrochemical determination of dopamine, uric acid and ascorbic acid using palladium nanoparticle-loaded carbon nanofibers modified electrode[J]. Biosens Bioelectron 24(4):632–637
12. Sun C, Lee H, Yang J et al (2011) The simultaneous electrochemical detection of ascorbic acid, dopamine, and uric acid using graphene/size-selected Pt nanocomposites[J]. Biosens Bioelectron 26(8):3450–3455
13. Zhang Y, Xia Z, Liu H et al (2013) Hemin-graphene oxide-pristine carbon nanotubes complexes with intrinsic peroxidase-like activity for the detection of H_2O_2 and simultaneous determination for Trp, AA, DA, and UA[J]. Sens Actuators B 188:496–501
14. Cui R, Wang X, Zhang G et al (2012) Simultaneous determination of dopamine, ascorbic acid, and uric acid using helical carbon nanotubes modified electrode[J]. Sens Actuators B 161(1):1139–1143
15. Savk A, Ozdil B, Demirkan B et al (2019) Multiwalled carbon nanotube-based nanosensor for ultrasensitive detection of uric acid, dopamine, and ascorbic acid[J]. Mater Sci Eng C 99:248–254
16. Ping J, Wu J, Wang Y et al (2012) Simultaneous determination of ascorbic acid, dopamine and uric acid using high-performance screen-printed graphene electrode[J]. Biosens Bioelectron 34(1):70–76
17. Zou HL, Li BL, Luo HQ et al (2015) A novel electrochemical biosensor based on hemin functionalized graphene oxide sheets for simultaneous determination of ascorbic acid, dopamine and uric acid[J]. Sens Actuators B 207:535–541
18. Wang C, Du J, Wang H et al (2014) A facile electrochemical sensor based on reduced graphene oxide and Au nanoplates modified glassy carbon electrode for simultaneous detection of ascorbic acid, dopamine and uric acid[J]. Sens Actuators B 204:302–309
19. Yang L, Liu D, Huang J et al (2014) Simultaneous determination of dopamine, ascorbic acid and uric acid at electrochemically reduced graphene oxide modified electrode[J]. Sens Actuators B 193:166–172
20. Sheng Z, Zheng X, Xu J et al (2012) Electrochemical sensor based on nitrogen doped graphene: Simultaneous determination of ascorbic acid, dopamine and uric acid[J]. Biosens Bioelectron 34(1):125–131
21. Wang C, Zou X, Zhao X et al (2015) Cu-nanoparticles incorporated overoxidized-poly (3-amino-5-mercapto-1,2,4-triazole) film modified electrode for the simultaneous determination of ascorbic acid, dopamine, uric acid and tryptophan[J]. J Electroanal Chem 741:36–41
22. Hsine Z, Blili S, Milka R et al (2020) Sensor based on redox conjugated poly(para-phenylene) for the simultaneous detection of dopamine, ascorbic acid, and uric acid in human serum sample[J]. Anal Bioanal Chem 412(18):4433–4446
23. Shieh Y, Lu Y, Wang T et al (2014) Electrocatalytic activities of Nafion/CdSe/Self-doped polyaniline composites to dopamine, uric acid, and ascorbic acid[J]. J Solid State Electrochem 18(4):975–984

24. Li YX, Lin XQ (2006) Simultaneous electroanalysis of dopamine, ascorbic acid and uric acid by poly (vinyl alcohol) covalently modified glassy carbon electrode[J]. Sens Actuators B 115(1):134–139
25. Niu XL, Yang W, Guo H et al (2012) A novel and simple strategy for simultaneous determination of dopamine, uric acid and ascorbic acid based on the stacked graphene platelet nanofibers/ionic liquids/chitosan modified electrode[J]. Talanta 99:984–988
26. Lai KF, Su WY, Chang WT et al (2013) The Synergic Effect of Conducting Polymer/Ionic Liquid Composite Electrodes on the Voltammetric Sensing of Biomolecules[J]. Int J Electrochem Sci 8(6):7959–7975
27. Rafati AA, Afraz A, Hajian A et al (2014) Simultaneous determination of ascorbic acid, dopamine, and uric acid using a carbon paste electrode modified with multiwalled carbon nanotubes, ionic liquid, and palladium nanoparticles[J]. Microchim Acta 181(15–16):1999–2008
28. Bagheri H, Pajooheshpour N, Jamali B et al (2017) A novel electrochemical platform for sensitive and simultaneous determination of dopamine, uric acid and ascorbic acid based on Fe_3O_4/SnO_2/Gr ternary nanocomposite[J]. Microchem J 131:120–129
29. Teymourian H, Salimi A, Khezrian S (2013) Fe_3O_4 magnetic nanoparticles/reduced graphene oxide nanosheets as a novel electrochemical and bioeletrochemical sensing platform[J], vol 49. Biosensors & Bioelectronics, pp 1–8
30. Zhang X, Zhang Y, Ma L (2016) One-pot facile fabrication of graphene-zinc oxide composite and its enhanced sensitivity for simultaneous electrochemical detection of ascorbic acid, dopamine and uric acid[J]. Sens Actuators B 227:488–496
31. Wang J, Nie P, Ding B et al (2017) Biomass derived carbon for energy storage devices[J]. J Mater Chem Mater energy Sustain 5(6):2411–2428
32. Zheng K, Li Y, Zhu M et al (2017) The porous carbon derived from water hyacinth with well-designed hierarchical structure for supercapacitors[J]. J Power Sources 366:270–277
33. Jiang L, Sheng L, Fan Z (2018) Biomass-derived carbon materials with structural diversities and their applications in energy storage[J]. Sci China Mater 61(2):133–158
34. Hadoun H, Sadaoui Z, Souami N et al (2013) Characterization of mesoporous carbon prepared from date stems by H3PO4 chemical activation[J]. Appl Surf Sci 280:1–7
35. Nahil MA, Williams PT (2012) Pore characteristics of activated carbons from the phosphoric acid chemical activation of cotton stalks[J], vol 37. Biomass & Bioenergy, pp 142–149
36. Huang YQ, Zang YJ, Ruan SJ et al (2021) A high efficiency N, P doped porous carbon nanoparticles derived from lotus leaves for simultaneous electrochemical determination of ascorbic acid, dopamine, and uric acid[J]. Microchem J 165:106152
37. Veeramani V, Madhu R, Chen S et al (2015) Biomass-derived functional porous carbons as novel electrode material for the practical detection of biomolecules in human serum and snail hemolymph[J]. Sci Rep 5(1):10141

38. Li XX, Li HY, Liu TT et al (2018) The biomass of ground cherry husks derived carbon nanoplates for electrochemical sensing[J]. Sens Actuators B 255:3248–3256
39. Zhang W, Liu L, Li Y et al (2018) Electrochemical sensing platform based on the biomass-derived microporous carbons for simultaneous determination of ascorbic acid, dopamine, and uric acid[J]. Biosens Bioelectron 121:96–103
40. Sha T, Liu J, Sun M et al (2019) Green and low-cost synthesis of nitrogen-doped graphene-like mesoporous nanosheets from the biomass waste of okara for the amperometric detection of vitamin C in real samples[J]. Talanta 200:300–306
41. Sudha V, Senthil Kumar SM, Thangamuthu R (2019) Hierarchical porous carbon derived from waste amla for the simultaneous electrochemical sensing of multiple biomolecules[J]. Colloids Surf B 177:529–540
42. Sha T, Li X, Liu J et al (2018) Biomass waste derived carbon nanoballs aggregation networks-based aerogels as electrode material for electrochemical sensing[J]. Sens Actuators B 277:195–204
43. Kim ND, Kim W, Joo JB et al (2008) Electrochemical capacitor performance of N-doped mesoporous carbons prepared by ammoxidation[J]. J Power Sources 180:671–675
44. Zhao D, Yu G, Tian K et al (2016) A highly sensitive and stable electrochemical sensor for simultaneous detection towards ascorbic acid, dopamine, and uric acid based on the hierarchical nanoporous PtTi alloy[J]. Biosens Bioelectron 82:119–126
45. Wang C, Du J, Wang H et al (2014) A facile electrochemical sensor based on reduced graphene oxide and Au nanoplates modified glassy carbon electrode for simultaneous detection of ascorbic acid, dopamine and uric acid[J]. Sens Actuators B 204:302–309
46. Thiagarajan S, Chen SM (2007) Preparation and characterization of PtAu hybrid film modified electrodes and their use in simultaneous determination of dopamine, ascorbic acid and uric acid[J]. Talanta 74(2):212–222
47. Prathap M, Srivastava R (2013) Tailoring properties of polyaniline for simultaneous determination of a quaternary mixture of ascorbic acid, dopamine, uric acid, and tryptophan[J]. Sens Actuators B 177:239–250
48. Safavi A, Maleki N, Moradlou O et al (2006) Simultaneous determination of dopamine, ascorbic acid, and uric acid using carbon ionic liquid electrode[J]. Anal Biochem 359(2):224–229
49. Zhao DY, Fan DW, Wang JP et al (2015) Hierarchical nanoporous platinum-copper alloy for simultaneous electrochemical determination of ascorbic acid, dopamine, and uric acid[J]. Microchim Acta 182(7–8):1345–1352
50. Zheng D, Ye JS, Zhou L et al (2009) Simultaneous determination of dopamine, ascorbic acid and uric acid on ordered mesoporous carbon/Nafion composite film[J]. J Electroanal Chem 625(1):82–87

Scheme 1

Scheme 1 is available in the Supplementary Files section

Figures

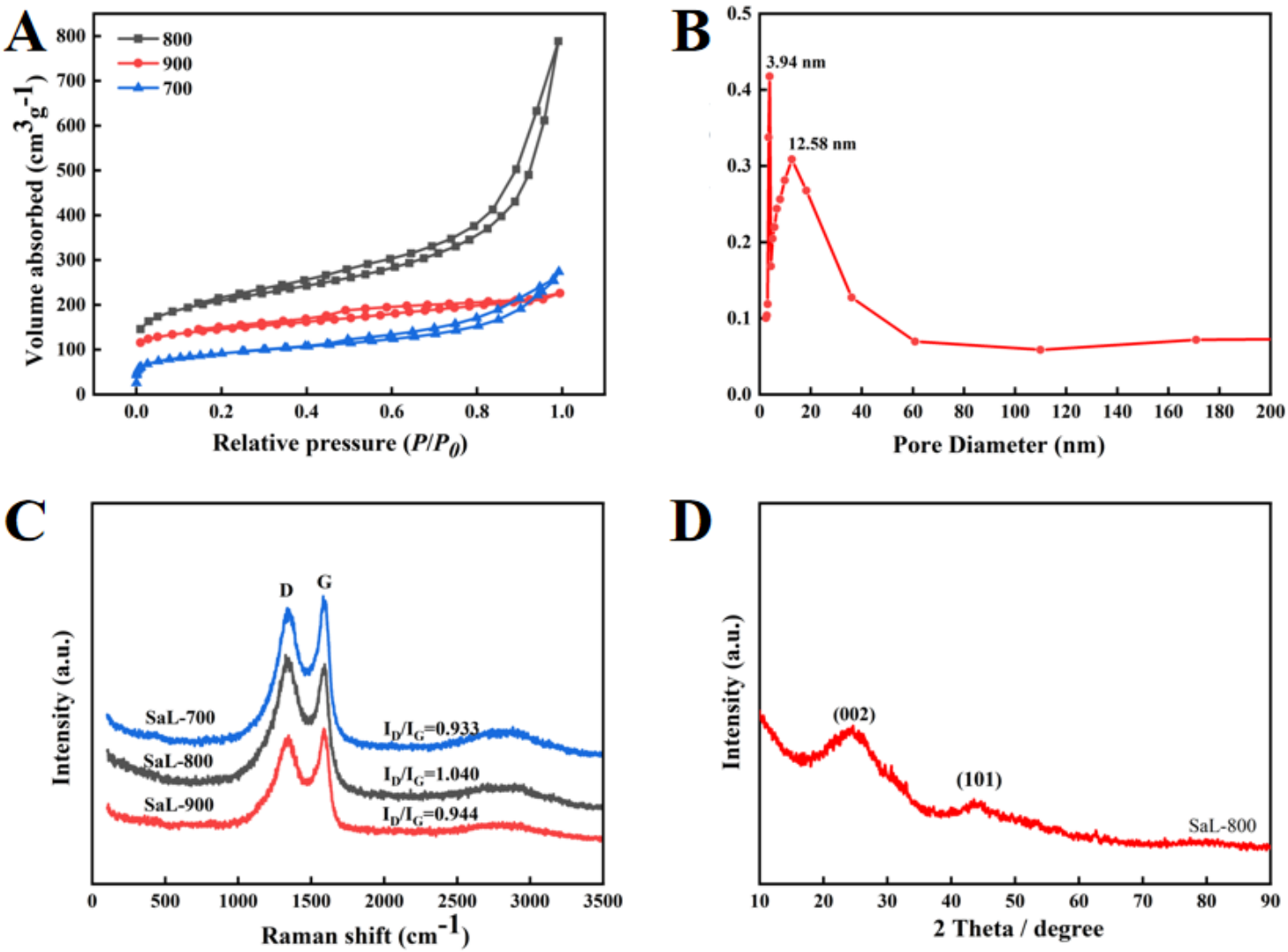

Figure 1

(A) Nitrogen adsorption-desorption curves of SaL-700, SaL-800 and SaL-900,

(B) pore size distribution of SaL-800, (C) Raman spectra of SaL-700, SaL-800 and SaL-900, (D) X-ray diffraction pattern of SaL-800

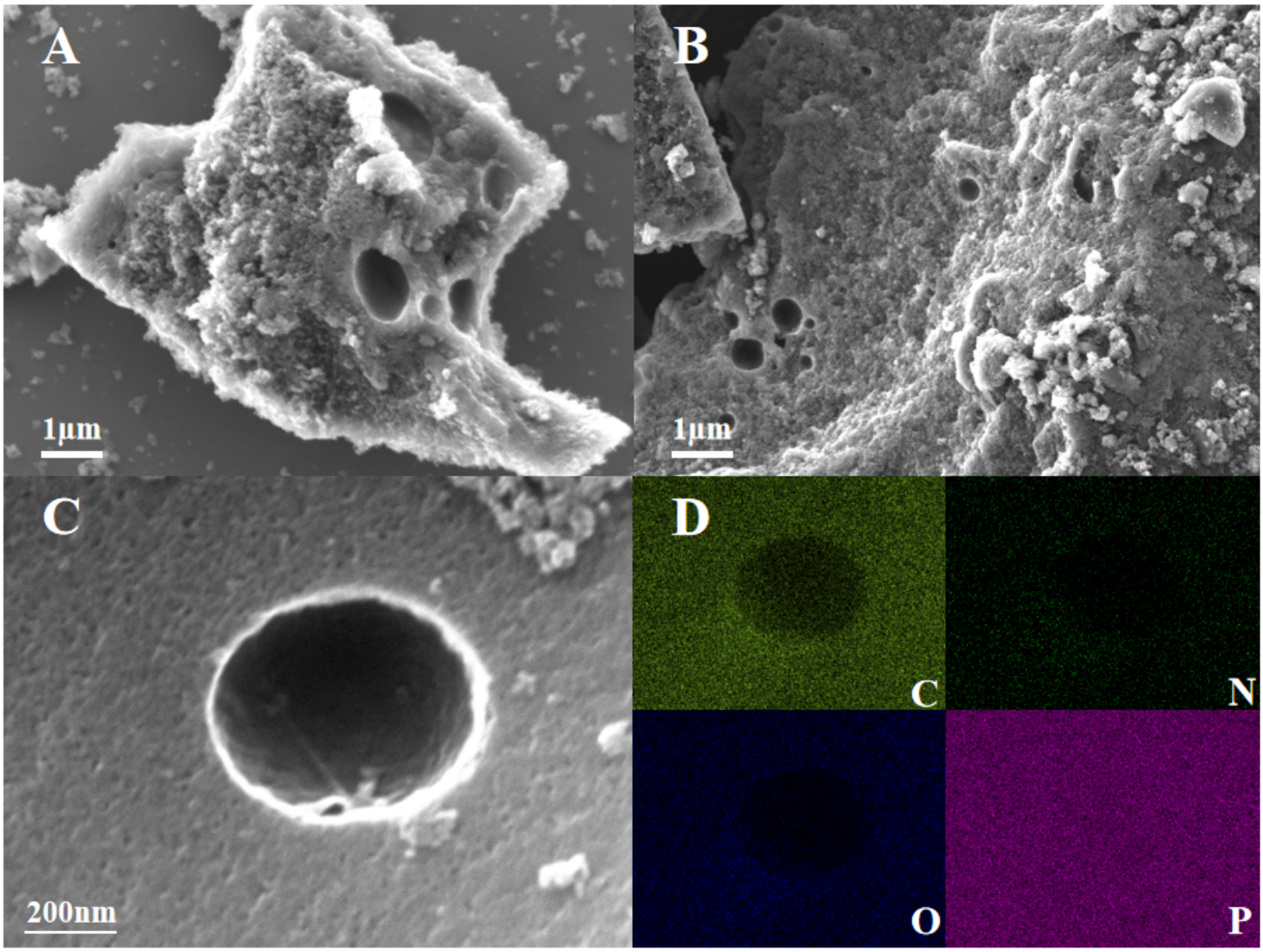

Figure 2

(A)-(C) The SEM characterization photographs of SaL-800,

(D) elemental mapping images of SaL-800

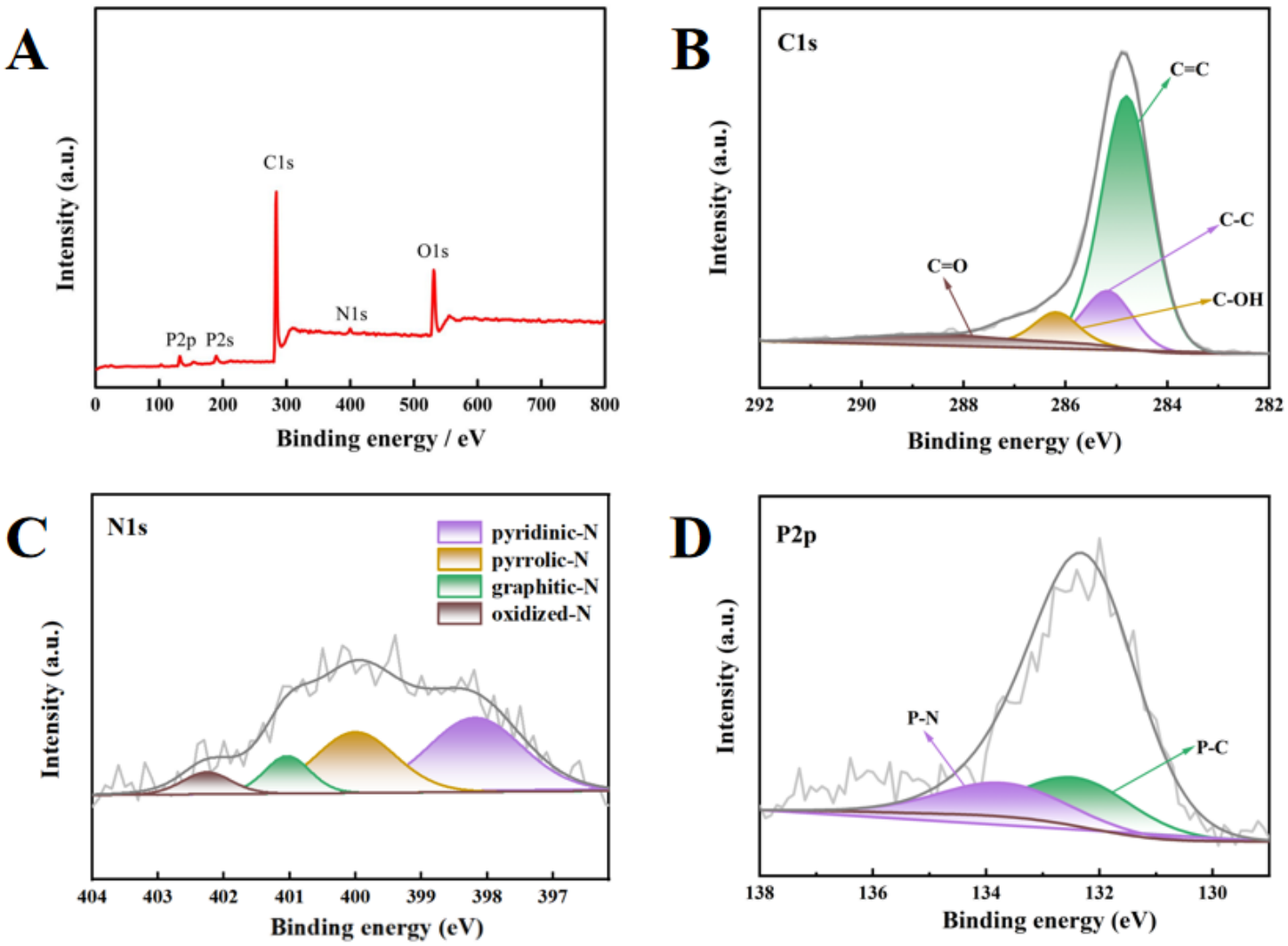

Figure 3

(A) The XPS full spectrum of SaL-800, (B) the high-resolution spectrums of C1s,

(C) N1s and (D) P2p

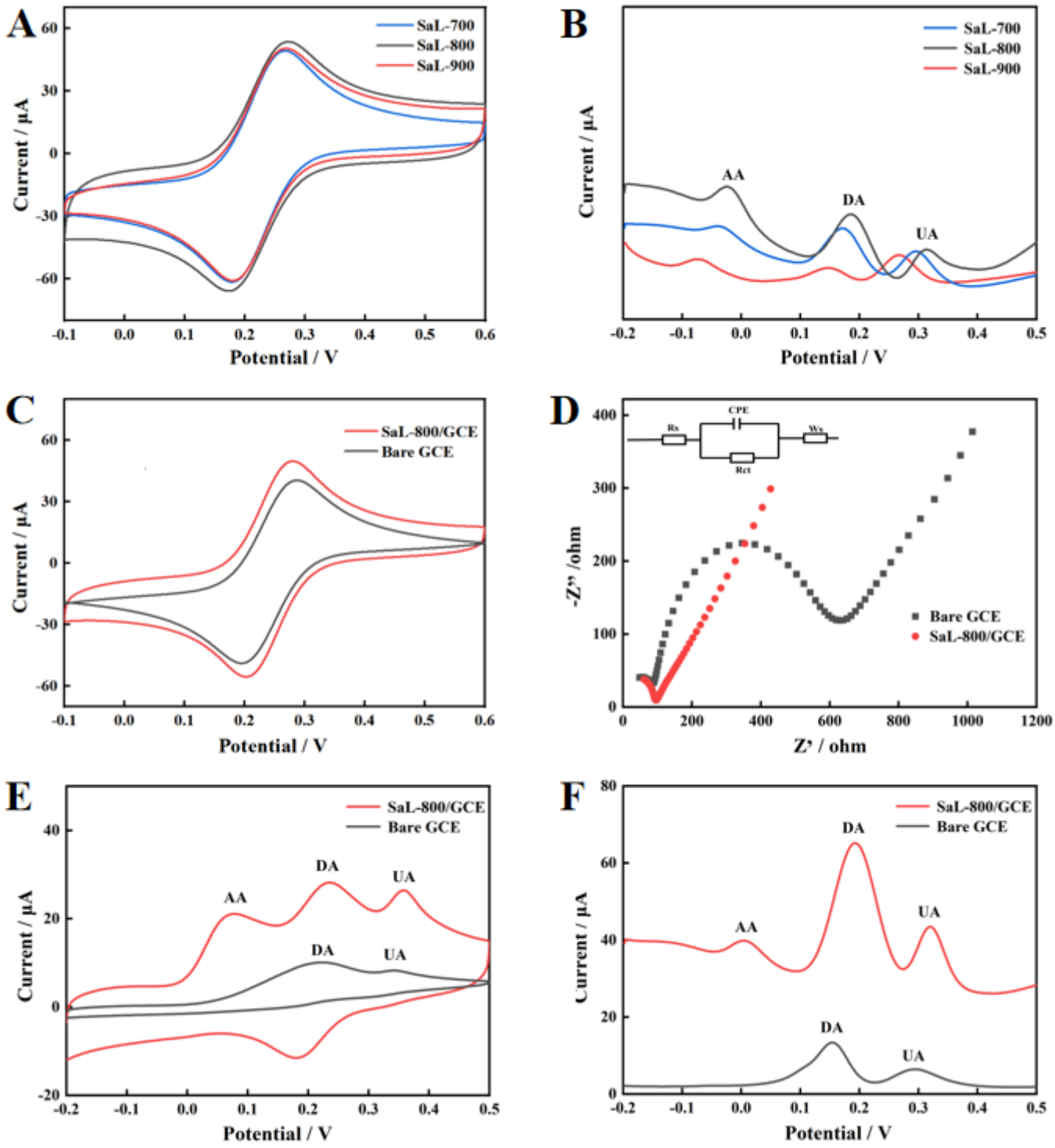

Figure 4

CV (A) and DPV voltammograms (B) of SaL-700, SaL-800 and SaL-900, CV(C), impedance and impedance fitting diagram (D) of Bare GCE and SaL-800/GCE, CV(E) and DPV voltammograms (F) of detecting AA, DA and UA at the same time

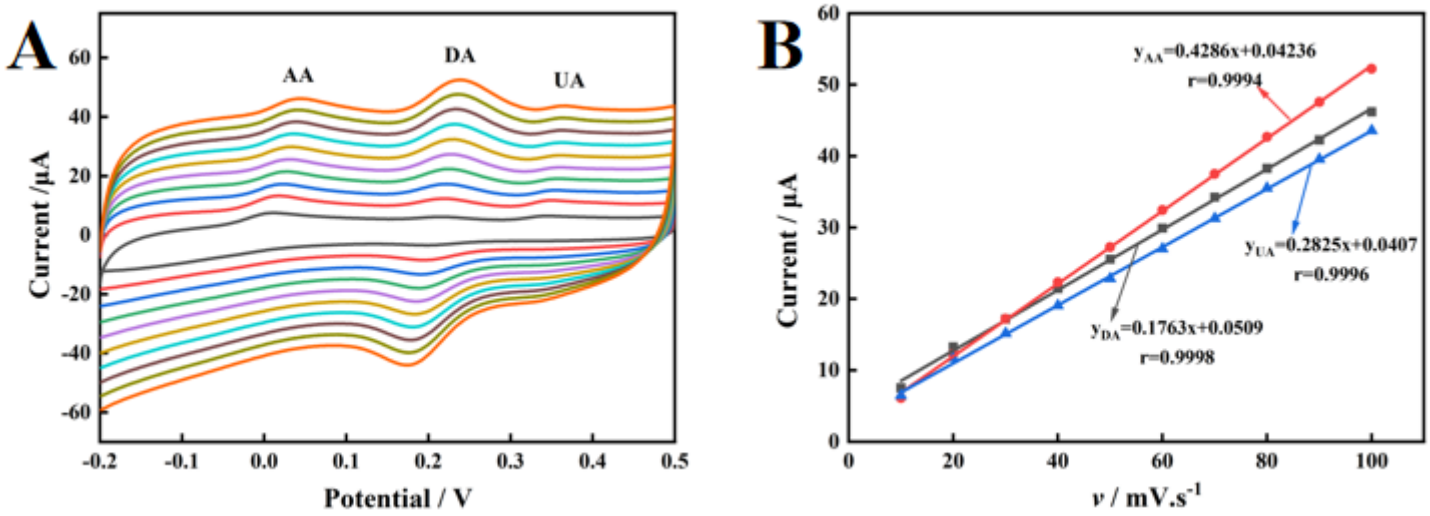

Figure 5

(A) The current signals of 500 μM AA , 50 μM DA and 50 μM UA in 0.1 M PBS mixed solution at different scanning rates, (B) relationships between anodic peak current of AA, DA and UA and scanning speeds

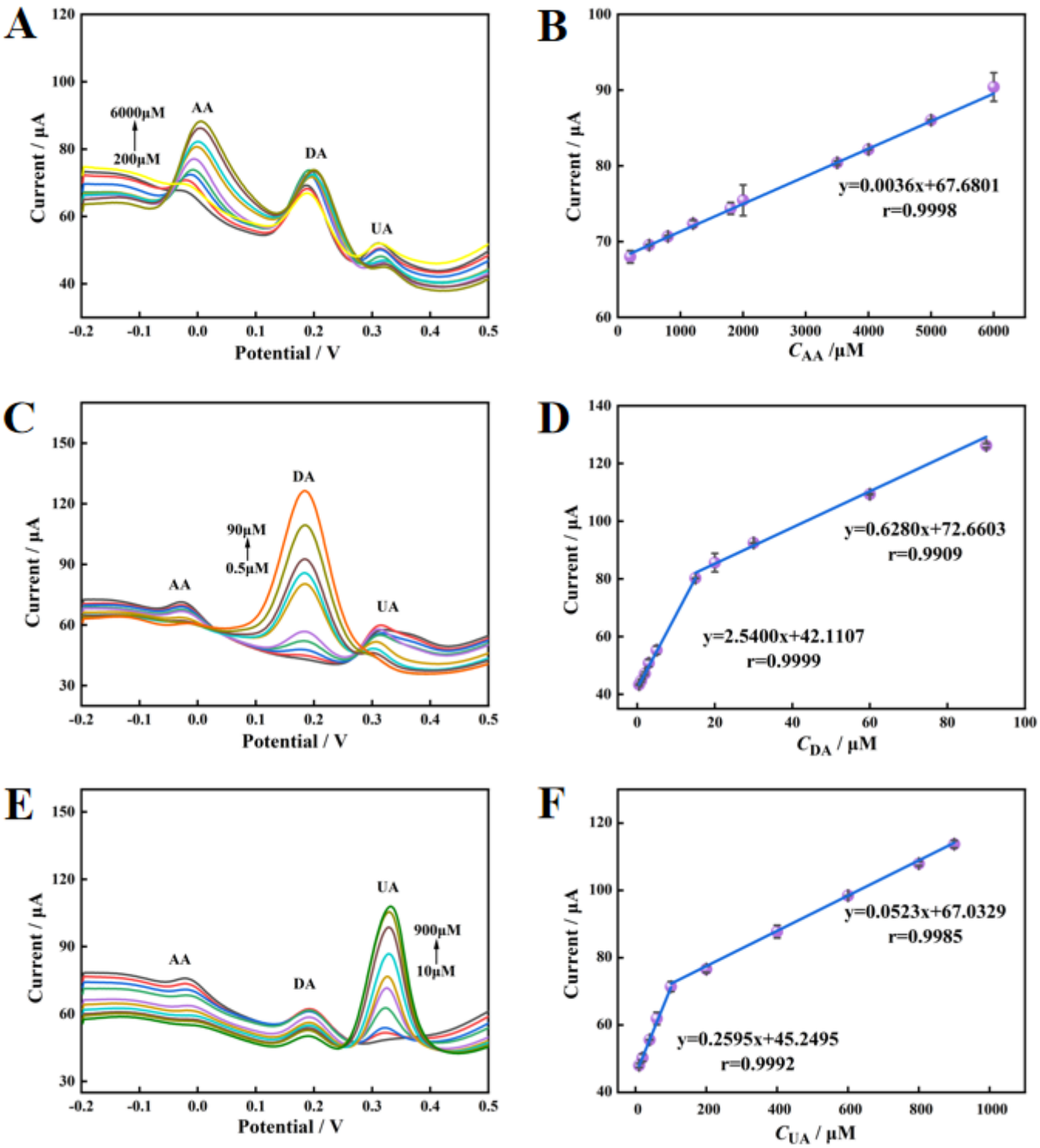

Figure 6

DPV diagrams of SaL-800/GCE in 0.1M PBS containing different concentrations of AA (A), DA (C) and UA (E) and corresponding fitting curves of AA (B), DA (D) and UA (F)

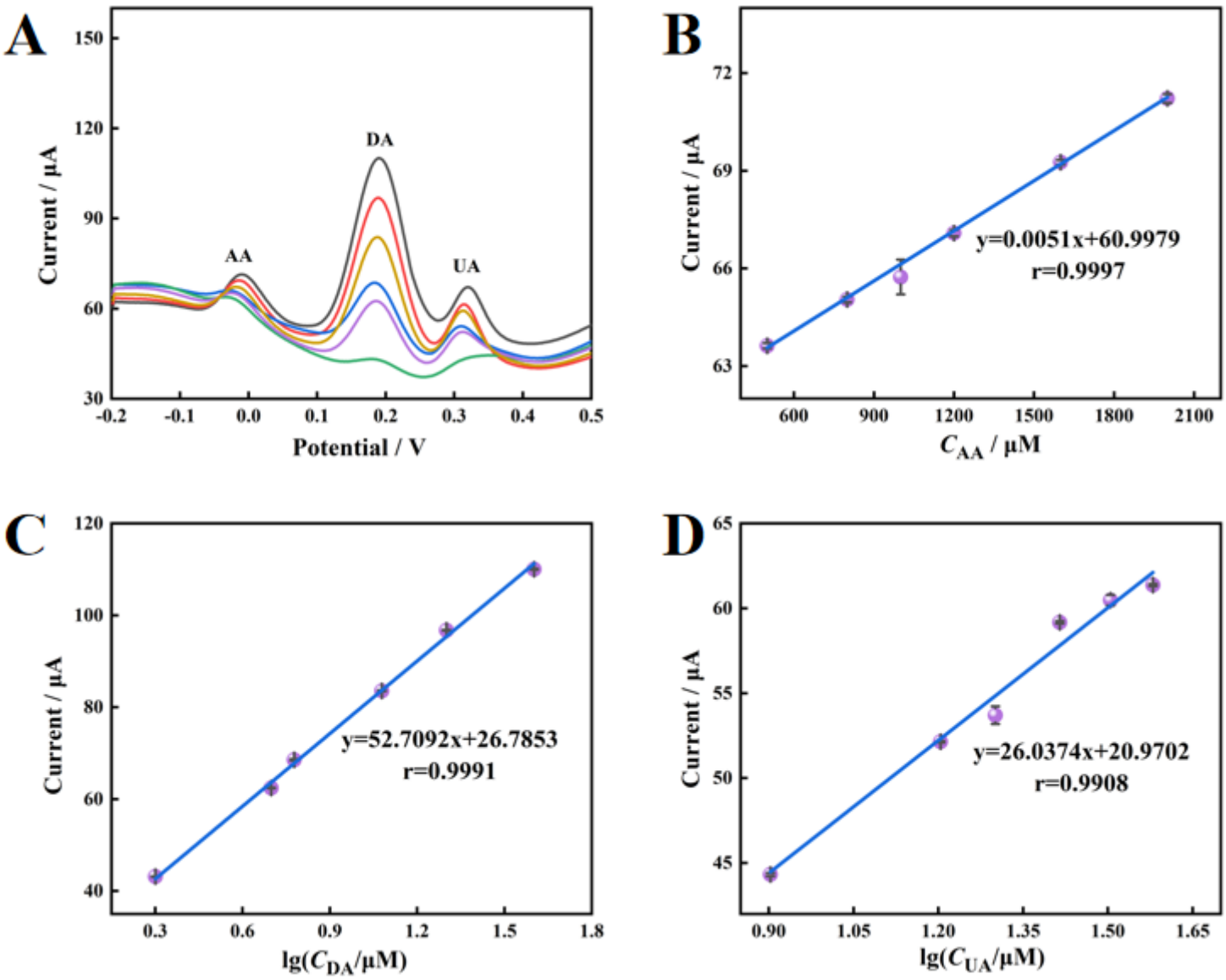

Figure 7

(A) DPV diagrams of simultaneous detection of AA, DA and UA by SaL-800/GCE, linear relationships between peak currents and concentrations of AA(B), DA (C)and UA(D)

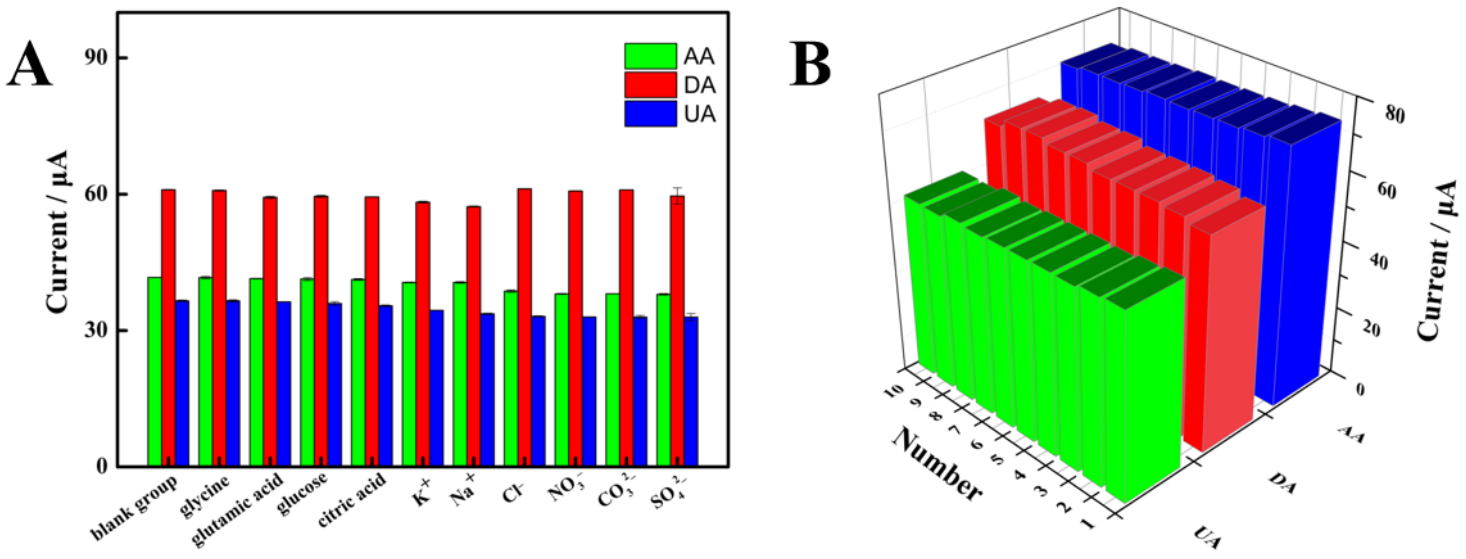

Figure 8

(A) The study on anti-interference ability of SaL-800/GCE, (B) reproducibility

Supplementary Files

This is a list of supplementary files associated with this preprint. Click to download.

- Scheme1.png
- SupplementaryMaterials.docx